Carbohydrate Polymers 95 (2013) 32–40

Contents lists available at SciVerse ScienceDirect

Carbohydrate Polymers

journal homepage: www.elsevier.com/locate/carbpol

Chemically and mechanically isolated nanocellulose and their self-assembled structures

Feng Jiang, You-Lo Hsieh*

Fiber and Polymer Science, University of California, Davis, CA 95616, USA

ARTICLE INFO

Article history:
Received 16 November 2012
Received in revised form 5 January 2013
Accepted 9 February 2013
Available online 28 February 2013

Keywords:
Cellulose nanocrystals
Cellulose nanofibrils
Rice straw
Self-assembly
Cellulose Iβ

ABSTRACT

Cellulose nanocrystals (CNCs) and nanofibrils (CNFs) have been isolated from pure rice straw cellulose via sulfuric acid hydrolysis, mechanical blending and TEMPO-mediated oxidation to 16.9%, 12% and 19.7% yields, respectively. Sulfuric acid hydrolysis produced highly crystalline (up to 90.7% CrI) rod-like (3.96–6.74 nm wide, 116.6–166 nm long) CNCs with similarly negative surface charges (−67 to −57 mV) and sulfate contents but decreasing yields and dimensions with longer hydrolysis time. Mechanical defibrillated CNFs were 82.5% crystalline and bimodally distributed in sizes (2.7 nm wide and 100–200 nm long; 8.5 nm wide and micrometers long). TEMPO mediated oxidation liberated the most uniform, finest (1.7 nm) and micrometer long, but least crystalline (64.4% CrI) CNFs. These nanocellulose self-assembled into submicron (153–440 nm wide) fibers of highly crystalline (up to 90.9% CrI) cellulose Iβ structure upon rapid freezing (−196 °C) and freeze-drying. The self-assembling behaviors were analyzed based on nanocellulose dimensions, specific surfaces and surface chemistries.

1. Introduction

Cellulose, synthesized by many organisms including plants, marine animals, fungi and bacteria as an important structural component, is the most abundant polymer in nature and has long been a major renewable source of materials. In the native forms, the long poly(β-1,4-glucopyranose) chains are organized in highly crystalline 1.5–3.5 nm wide nanofibrils with intramolecular and intermolecular hydrogen bonds as part of larger microfibrils and macroscopic fibers (Habibi, Lucia, & Rojas, 2010; Klemm, Heublein, Fink, & Bohn, 2005). The nanofibrillar domains, generally referred as nanocellulose, can be separated from each other by overcoming the extensive and strong inter-fibrillar hydrogen bonds with harsh caustic chemicals, specific enzymes and/or intense mechanical forces. Nanocellulose, either in rod-like cellulose nanocrystals (CNCs) or longer cellulose nanofibrils (CNFs), has generated significant interest due to its nanoscale dimensions and superior properties including extraordinary elastic modulus of 150 GPa (Iwamoto, Kai, Isogai, & Iwata, 2009), low axial thermal expansion coefficient of 10^{-7} K^{-1} (Nishino, Matsuda, & Hirao, 2004) and high specific surface area (Heath & Thielemans, 2010; Saito, Uematsu, Kimura, Enomae, & Isogai, 2011).

Acid hydrolysis has been the primary method for isolating rod-like CNCs since early reports in the late 1940s (Nickerson & Habrle, 1947). Sulfuric acid hydrolysis has shown to produce relatively uniformly sized CNCs from a single source under a fixed condition, however, widely varied dimensions of 3–70 nm widths and 35–3000 nm lengths have been reported from different cellulose sources and hydrolysis conditions (Beck-Candanedo, Roman, & Gray, 2005; Elazzouzi-Hafraoui et al., 2008; Habibi et al., 2010). Other acids such as hydrochloric acid, hydrobromic acid as well as mixed acetic and nitric acids are also capable of hydrolyzing cellulose into CNCs, without esterifying the surfaces as in the case with sulfuric acid while in higher yields (Jiang, Esker, & Roman, 2010; Sadeghifar, Filpponen, Clarke, Brougham, & Argyropoulos, 2011; Zuluaga, Putaux, Restrepo, Mondragon, & Ganan, 2007). Strong acids hydrolyze cellulose chains in the less ordered regions, producing CNCs with higher crystallinities than the original source but usually at low yields of less than 30% (Bondeson, Mathew, & Oksman, 2006; Lu & Hsieh, 2012). A variety of mechanical defibrillation methods including high-pressure homogenization (Zimmermann, Bordeanu, & Strub, 2010), grinding (Abe & Yano, 2009), ultrasonication (Chen, Yu, & Liu, 2011), cryocrushing (Alemdar & Sain, 2008) and high-speed blending (Uetani & Yano, 2011) have shown to improve the yields, some to as high as 100% (Isogai, Saito, & Fukuzumi, 2011). These mechanical processes produce longer (several micrometers) but less uniformly sized (5–100 nm wide) (Siro & Plackett, 2010) and less crystalline (Iwamoto, Nakagaito, & Yano, 2007) CNFs. More uniform CNFs with 1–5 nm diameters have been isolated through oxidation using nitroxyl radical 2,2,6,6-tetramethylpyperidine-1-oxyl (TEMPO) (Saito, Nishiyama, Putaux, Vignon, & Isogai, 2006). The TEMPO oxidized CNFs have been reported to have the same crystallinity as the starting materials (Saito, Kimura, Nishiyama, &

* Corresponding author. Tel.: +1 530 752 0843.
E-mail address: ylhsieh@ucdavis.edu (Y.-L. Hsieh).

0144-8617/$ – see front matter © 2013 Elsevier Ltd. All rights reserved.
http://dx.doi.org/10.1016/j.carbpol.2013.02.022

Isogai, 2007) and, when aided with mechanical means, over 90% yield (Isogai et al., 2011).

Rice straw is the largest crop residue globally and, with relatively high cellulose contents of ca. 40% (Lu & Hsieh, 2012), is a significantly under-utilized, non-wood cellulose source. Rice straw cellulose has been mechanically ground to 12–35 nm wide and several micrometer long nanofibrils with very similar crystal structures and mechanical properties as those from grinding wood and potato tuber (Abe & Yano, 2009). Sulfuric acid hydrolysis of rice straw cellulose, on the other hand, produced more uniformly sized CNCs, i.e., averaged 11.2 nm wide, 5.06 nm thick and 117 nm long, but at a very low 6% yield (Lu & Hsieh, 2012).

Furthermore, in freeze-drying these CNC suspensions to solid forms, cellulose nanocrystals were observed to self-assemble into micrometer-long, highly crystalline (91.2%) and nonporous or macroporous fibers with an average diameter of 386 nm that remained in the assembled fibrous form in suspensions with hand shaking and mechanical stirring for prolonged time (Lu & Hsieh, 2012). Cellulose nanofibers have been generated by electrospinning of cellulose and cellulose derivative solutions (Liu & Hsieh, 2002), a process relying on chemicals in dissolution and derivatization of cellulose which resulting in the loss of the native cellulose Iβ crystalline structure. The intriguing self-assembling behavior of CNCs suggests this cryogenic process to be an attractive non-chemical alternative for fabricating ultra-fine cellulose fibers from aqueous nanocellulose suspensions while achieving highest crystallinity surpassing even its source.

This study was to isolate nanocellulose from rice straw cellulose by different individual isolation approaches, to characterize nanocellulose structures in relationship to each isolation method as well as with each other and to investigate their self-assembling behaviors during rapid freezing and freeze-drying. Sulfuric acid hydrolysis, TEMPO-mediated oxidization and mechanical blending were individually applied to pure rice straw cellulose to isolate nanocellulose. The different forms of nanocellulose, i.e., CNCs and CNFs, and their yields, chemical and crystalline structures, thermal stability, physical dimensions, morphologies and surface properties were analyzed and compared. This represented the first report of TEMPO oxidation of rice straw cellulose as well as systematic comparisons of nanocellulose from a single and significant rice straw feedstock.

2. Experimental

2.1. Materials

Pure cellulose was isolated from rice straw (Calrose variety) by a three-step process of 2:1 v/v toluene/ethanol extraction, acidified $NaClO_2$ dissolution of lignin (1.4%, 70 °C, 5 h) and alkaline dissolution of hemicellulose and silica (5% KOH, 90 °C for 2 h) to a 36% yield (Lu & Hsieh, 2012). Sulfuric acid (H_2SO_4, 95–98%, ACS GR, EMD), hydrochloric acid (HCl, 1 N, Certified, Fisher Scientific), sodium hydroxide (NaOH, 1 N, Certified, Fisher Scientific), sodium hypochlorite (NaClO, 11.9%, reagent grade, Sigma–Aldrich), 2,2,6,6-tetramethylpyperidine-1-oxyl (TEMPO, 99.9%, Sigma–Aldrich), sodium bromide (NaBr, BioXtra, 99.6%, Sigma–Aldrich) were used as received without further purification. All water used was purified by Milli-Q plus water purification system (Millipore Corporate, Billerica, MA).

2.2. Nanocellulose isolation

2.2.1. Cellulose nanocrystals (CNCs) by sulfuric acid hydrolysis

Rice straw cellulose was added to preheated (45 °C) sulfuric acid (64 wt%) at a 8.75 mL/g acid-to-cellulose ratio and proceeded at 45 °C under constant stirring for 15, 45 and 60 min. Hydrolysis was terminated by quenching with 10-fold cold water and the suspension was centrifuged (5000 rpm, 15 min) to collect the sediment which was dialyzed against water until neutral. Further centrifugation (5000 rpm, 30 min) yielded the supernatant as CNC suspension and the sediments consisting cellulose fragments from incomplete hydrolysis. The CNC suspension was then ultrasonicated in an ice bath for 5 min at 40% amplitude to disperse CNCs (Misonix ultrasonic liquid processors S4000), then filtered through 2 μm pore size syringe filter (Whatman Puradisc™ 25GD). The yields of CNCs were calculated gravimetrically based on the original pure rice straw cellulose and reported as percentages. The CNCs were referred as CNC15, CNC45 and CNC60 for the 15, 45 and 60 min reactions, respectively.

2.2.2. Cellulose nanofibrils by high-speed blending (CNF-B)

Cellulose nanofibrils were mechanically defibrillated from rice straw cellulose using a high-speed blender (Vitamix 5200) in three consecutive blending and separation steps. Cellulose (0.5 g) was added to 200 mL water and mixed with magnetic stirring bar for 5 min. The cellulose suspension was transferred to a 2L blender beaker and blended at 37,000 rpm for 60 min, reaching 97 °C. The suspension was cooled to room temperature, then centrifuged (1500 rpm, 15 min) to collect the first CNF-containing supernatant, referred as CNF-B60. The first precipitate was re-dispersed in 200 mL water and blended for another 30 min and centrifuged to obtain a second CNF-containing supernatant that was blended for a total of 90 min, referred as CNF-B90. The second precipitate was re-dispersed, blended for 30 min and centrifuged to obtain a third CNF-containing supernatant or CNF-B120. The final precipitate was referred as blended cellulose fibers (CF-B). The yields were calculated gravimetrically and cumulative yields were used to for CNF-B90 and CNF-B120. All three CNF-B supernatant were combined, concentrated in a rotary evaporator and designated as CNF-B for further characterization.

2.2.3. Cellulose nanofibrils by TEMPO mediated oxidation (CNF-T)

Cellulose (1.0 g) was added to 100 mL water and mixed with a magnetic stirrer for 5 min, then 2 mL of an aqueous mixture of TEMPO (0.016 g) and sodium bromide (0.1 g) was added and stirred for another 5 min. Oxidation reaction was initiated by adding 11.9% NaClO solution drop-wisely to reach 5 mmol NaClO per gram of cellulose. The pH decreased as oxidation proceeded and was adjusted to 10 ± 0.2 with 0.5 M NaOH. The oxidation reaction ended when no acid was produced or pH ceased to lower, lasting approximately 65 min. The pH was adjusted to 7 with 0.5 M HCl. The suspension was centrifuged (5000 rpm, 15 min), dialyzed against water and centrifuged (1500 rpm, 15 min) again to obtain the CNF-containing supernatant which was then concentrated using a rotary evaporator, ultrasonicated at 40% amplitude for 5 min in an ice bath, then filtered (Whatman 541) to remove large particulates. It should be noted that TEMPO oxidation was conducted without being aided by any other means of mechanical forces to study its sole ability to isolate cellulose nanofibrils. CNF prepared by TEMPO oxidation was named as CNF-T, and the yield was calculated gravimetrically. The final precipitate was also collected and referred as TEMPO oxidized cellulose fiber (CF-T).

2.3. Characterization

All aqueous suspensions were stored at 4 °C before surface charge and zeta potential characterization and imaging upon drying on specified substrates. Rapid freezing of 20 mL of dilute aqueous suspensions and precipitates, i.e., 0.1 wt% CNCs, CF-Ts, CNF-Ts and CF-Bs or 0.05 wt% CNF-Bs, was conducted by immersing each in 50 mL centrifuge tube in liquid nitrogen (−196 °C) and lyophilized

at −50 °C in a freeze-drier (FreeZone 1.0L Benchtop Freeze Dry System, Labconco, Kansas City, MO). All solids rapidly frozen in liquid nitrogen and freeze-dried are referred as "freeze-dried" from here on for brief.

2.3.1. Zeta potential measurement

The zeta potential (ζ, mV) of 0.1 wt% aqueous CNC and CNF-T suspensions was measured without ionic strength adjustment using a Zetasizer Nano S90 (Malvern Instrument). The ζ value was calculated from the electrophoretic mobility for each suspension using Henry equation and Huckel approximation validated for $ka \ll 1$, where k is inverse of Debye length and a is the nanoparticle radius (Uetani & Yano, 2012). Three measurements were conducted for each suspension and the mean and standard deviation were reported.

2.3.2. Atomic force microscopy (AFM)

For AFM imaging, 10 μL of 0.002 wt% suspension was deposited onto a freshly cleaved mica surface, air-dried and scanned using an Asylum-Research MFP-3D atomic force microscope under ambient condition under the tapping mode with OMCL-AC160TS standard silicon probes. The scan rate was set to 1 Hz and image resolution is 512 × 512 pixels. The average heights were determined from the height profiles of over 300 particles with MFP3D 090909 + 1409 plugin in IGOR Pro 6.21.

2.3.3. Transmission electron microscopy (TEM)

Either CNC or CNF suspension (0.01 wt%, 8 μL) was deposited onto glow-discharged carbon-coated TEM grids (300-mesh copper, formvar-carbon, Ted Pella Inc., Redding, CA) and the excess liquid was removed by blotting with a filter paper after 10 min. The specimens were then negatively stained with 2% uranyl acetate solution for 5 min, blotted to remove excess solution and allowed to dry under the ambient condition. The samples were observed using a Philip CM12 transmission electron microscope operated at a 100 kV accelerating voltage. The lengths of CNCs and CNFs were measured and calculated from over 200 samples using analySIS FIVE software.

2.3.4. Scanning electron microscopy (SEM)

Rice cellulose, freeze-dried CNCs and CNFs were mounted with conductive carbon tape and sputter coated with gold. For imaging CF-B and CF-T, 10 μL of 0.1 wt% suspension was deposited on cleaned silicon wafer and air-dried. The silicon wafers were mounted and coated with carbon. The prepared samples were imaged by a field emission scanning electron microscope (FE-SEM) (XL 30-SFEG, FEI/Philips, USA) at a 5-mm working distance and 5-kV accelerating voltage. Widths of freeze-dried fibers were measured from 50 individual fibers.

2.3.5. Fourier transform infrared spectroscopy (FTIR)

FTIR spectra of pure rice cellulose, freeze-dried CNCs and CNFs as transparent KBr pellets (1:100, w/w) were obtained from a Thermo Nicolet 6700 spectrometer. The spectra were collected at ambient conditions in the transmittance mode from an accumulation of 128 scans at a 4 cm^{-1} resolution over the regions of 4000–400 cm^{-1}.

2.3.6. X-ray diffraction (XRD)

XRD spectra for pure rice cellulose, freeze-dried CNCs and CNFs were collected on a Scintag XDS 2000 powder diffractometer using a Ni-filtered Cu Kα radiation (λ = 1.5406 Å) at an anode voltage of 45 kV and a current of 40 mA. Freeze-dried solids were compressed between two glass slides into flat sheets with around 1 mm thickness. Diffractograms were recorded from 5° to 40° at a scan rate of 2°/min. Crystallinity index (*CrI*) was calculated from the intensity of the 2 0 0 peak (I_{200}, $2\theta = 22.6°$) and the intensity minimum between the peaks at 2 0 0 and 110 (I_{am}, $2\theta = 18.7°$) by using the empirical equation (Segal, Creely, Martin, & Conrad, 1959).

$$CrI = \frac{I_{200} - I_{am}}{I_{200}} \times 100 \quad (1)$$

The crystallite dimensions of these samples were calculated using Scherrer equation (Scherrer, 1918),

$$D_{hkl} = \frac{0.9\lambda}{\beta_{1/2} \cos\theta} \quad (2)$$

where D_{hkl} is the crystallite dimension in the direction normal to the hkl lattice planes, λ is the X-ray radiation wavelength (1.5406 Å), $\beta_{1/2}$ is the full width at half-maximum of the diffraction peak, and θ is the corresponding Bragg angle. $\beta_{1/2}$ was determined from Voigt profile fits of the diffraction peaks calculated with PeakFit (v4.12, Systat Software, Inc.).

2.3.7. Thermogravimetric analysis (TGA)

TGA analyses of rice straw cellulose and freeze-dried CNCs and CNFs were performed on a TGA-50 thermogravimetric analyzer (Shimadzu, Japan). Each sample (5 mg) was heated at 10 °C/min from 25 °C to 500 °C under purging N_2 (50 mL/min).

3. Results and discussion

3.1. Nanocellulose yields

Pure rice straw cellulose was hydrolyzed into cellulose nanocrystals (CNCs) by sulfuric acid hydrolysis as well as defibrillated into cellulose nanofibrils (CNFs) by either high-speed blending (CNF-B) or TEMPO-mediated oxidation (CNF-T). The CNC yields were 16.9% (CNC15), 6.8% (CNC45) and 4.9% (CNC60) from sulfuric acid hydrolysis for 15, 45 and 60 min, respectively. The decreasing yields with longer reaction time is expected as cellulose chains in the less ordered regions are hydrolyzed to separate the crystalline domains that reduce in sizes as the surface chains are further hydrolyzed, while cellulose fragments are broken into soluble oligo- and mono-saccharides. The 16.9% yield of CNC15 shows that sulfuric acid hydrolysis for as short as 15 min are sufficient to release CNCs from rice straw cellulose under the current condition (64 wt% H_2SO_4, 45 °C).

Mechanical defibrillation yielded 4.8%, 8.8% and 12.0% CNF-Bs after 60, 90 and 120 min of blending, respectively. The yields increased significantly by 83% and 150% with the additional times, validating the effectiveness of two additional blending and separation. However, the total CNF yield of 12.0% from three consecutive blending steps over a total of 2 h is lower than that of CNCs from 15 min sulfuric acid hydrolysis. In contrast, TEMPO-mediated oxidation alone yielded 19.7% CNF-Ts, higher than both sulfuric acid hydrolysis (16.9% CNCs) and mechanical defibrillation (12.0% CNF-Bs).

3.2. Nanocellulose morphologies

3.2.1. CNCs isolated by sulfuric acid hydrolysis

AFM height images of CNC15 showed both nanorods and abundant naoparticles whereas only uniformly shaped nanorods were observed for CNC45 and CNC60 (Fig. 1a,d,g), the latter two similar to those isolated from sulfuric acid hydrolysis of cellulose from other sources (Beck-Candanedo et al., 2005; Dong & Roman, 2007; Elazzouzi-Hafraoui et al., 2008). AFM height profiles and distribution showed CNC15 nanoparticles and nanorods to be 2.13 ± 0.72 nm and 6.74 ± 1.84 nm thick, respectively (Fig. 1b and c). Longer hydrolysis reduced the average thickness of CNC45 (Fig. 1e and f) and CNC60 (Fig. 1h and i) nanorods to 4.72 ± 1.25 nm and 3.96 ± 1.32 nm, respectively. The observation of both nanoparticles

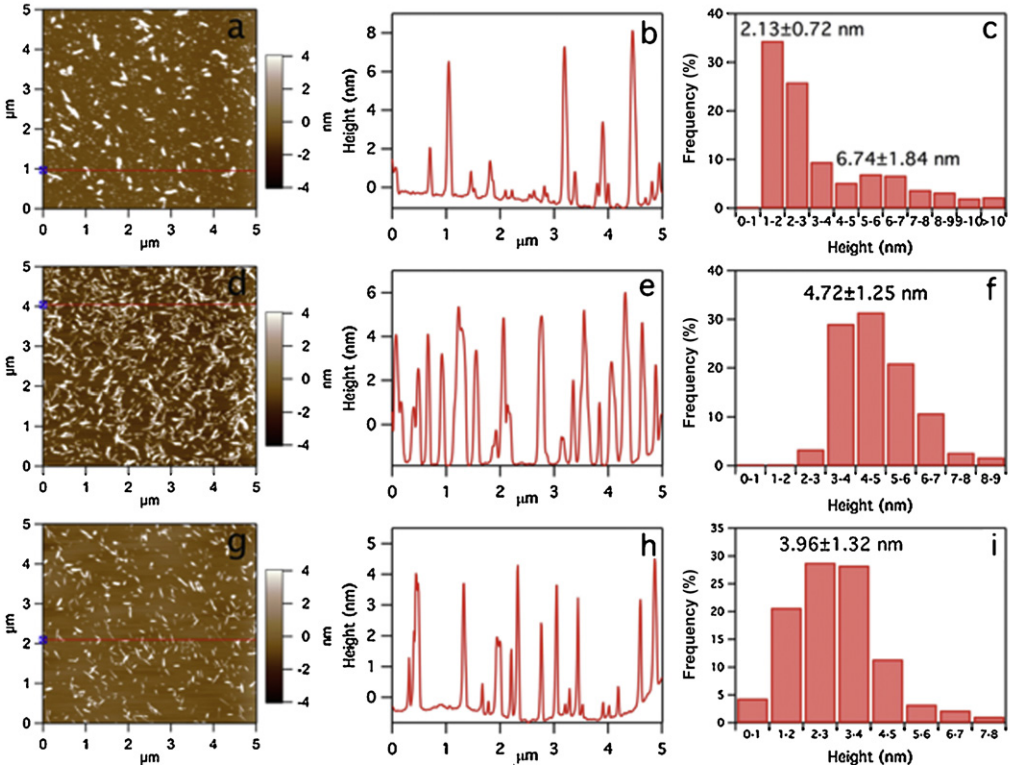

Fig. 1. AFM of CNC15 (a,b,c), CNC45(d,e,f) and CNC60 (g,h,i): (a,d,g) height images, (b,e,h) height profiles along lines in a, d, g, and (c,f,i) lateral dimension distribution.

and nanorods in CNC15 shows more heterogeneous morphologies in the initial stage of hydrolysis. As hydrolysis progresses, the nanorods reduced in lateral dimensions while the smaller nanoparticles were broken down to soluble mono- and/or oligosaccharides. The disappearance of numerous 2 nm nanoparticles and the reduced dimension of CNC45 are consistent with the significantly lowered 6.8% yield as compared to the 16.9% yield of CNC15. Lengthening the hydrolysis time to 60 min reduced both nanorod size and yield further.

The presence of both CNC15 nanoparticles and nanorods and more uniformly sized CNC45 and CNC60 nanorods were further confirmed by TEM observations (Fig. 2a–c). CNC15 nanorods appeared to be bimodally distributed to in lengths of 68.6 ± 16.6 nm and 165.6 ± 42.0 nm (Fig. 2a). CNC45 (Fig. 2b) and CNC60 (Fig. 2c) were shorter than CNC15, averaging 143.3 ± 30.9 nm and 116.6 ± 27.6 nm in lengths, respectively. CNC60 also appeared narrower than CNC45, again consistent with the AFM height values. The bright spherical particles in Fig. 2a and b are staining artifacts from TEM sample preparation and irrelevant to CNCs. Both AFM and TEM images confirmed that, although a higher yield of 16.9% was achieved at 15 min, CNC15 contained heterogeneous morphologies of both nanoparticles and bimodally sized nanorods. The CNC nanorods exhibited reduced widths (6.74 nm, 4.72 nm, 3.96 nm) and lengths (165.6 nm, 143.3 nm, 116.6 nm) with increasing hydrolysis time. More uniform CNCs could be attained with longer hydrolysis time, such as 45 min, at a sacrificed yield of 6.8%.

3.2.2. *CNFs defibrillated by high-speed blending and TEMPO oxidation*

The AFM height image of CNF-Bs showed successful isolation of nanofibrils by simple high-speed blending (Fig. 3a). The CNF-Bs were bimodally distributed in dimensions with smaller ones averaging 2.70 ± 1.22 nm wide (Fig. 3c) and 100–200 nm long (Fig. 3a) and larger ones averaging 8.46 ± 4.14 nm wide (Fig. 3c) and several micrometers long (Fig. 3a and d). The presence of bimodally distributed CNF-Bs showed that mechanical defibrillation produced less uniformly sized CNFs that differed more in lengths by one order of magnitude.

TEMPO-mediated oxidation yielded nearly 20% CNF-Ts that appeared highly uniform in morphologies by AFM (Fig. 3d), with 90% of CNF-Ts less than 3 nm wide and an average width of 1.73 ± 0.56 nm (Fig. 3e and f). CNF-Ts are hundreds of nanometers to micrometer long, much smaller, narrower and more uniform than CNF-Bs (inset in Fig. 3a).

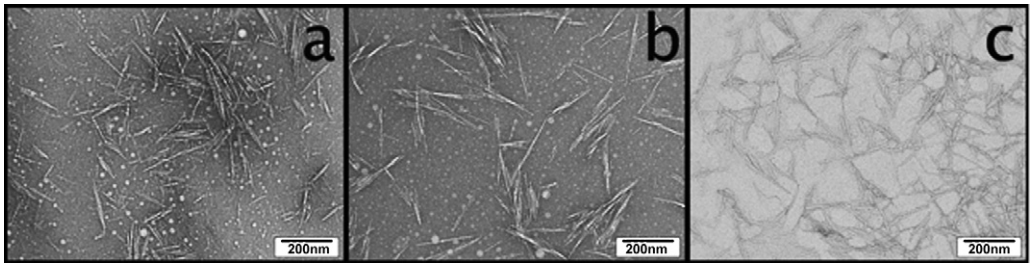

Fig. 2. TEM images of CNC15 (a), CNC45 (b) and CNC60 (c).

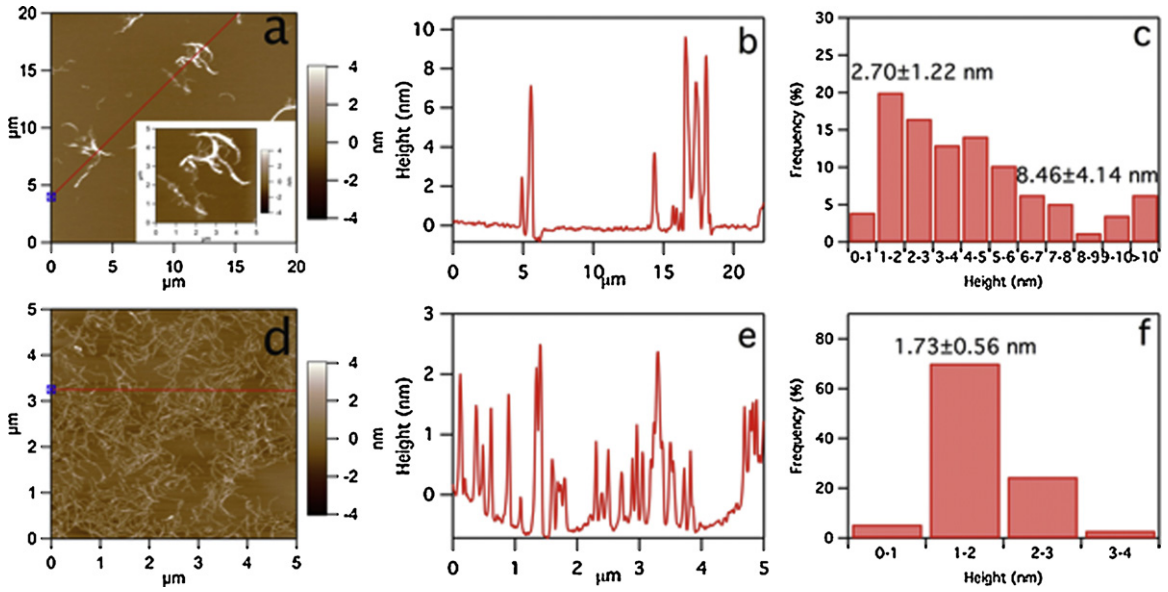

Fig. 3. CNF-B (a–c) and CNF-T (d–f): (a,d) AFM height image, (b,e) height profile along line in a and d, (c,f) height distribution.

3.3. Surface characteristics of nanocellulose

The surface charge of CNC15 determined by conductometric titration was 0.29 mmol/g cellulose (Fig. 1 in supplementary data). The atomic sulfur contents determined by EDS were 0.22%, 0.24% and 0.21% for CNC15, CNC45 and CNC60, respectively (Fig. 2 in supplementary data). The close sulfur content values suggest similar surface charges among these CNCs. The zeta potential, ζ, values for CNC15, CNC45 and CNC60 were -66.7 ± 0.3, -57.3 ± 2.7 and -63.8 ± 2.2 mV, respectively. These negative ζ values are consistent with the presence and similar contents of surface sulfate groups. CNF-Ts had a surface charge of 1.32 mmol/g cellulose (Fig. 1 in supplementary data) and a ζ values of -113.3 ± 1.5 mV, about twice of those of CNCs. Both conductometric titration and ζ value showed CNF-Ts to be far more polar and negatively charged than CNCs, clearly evident of significant amount of the more polar carboxyl groups on the TEMPO-oxidized nanofibril surfaces.

The 0.29 mmol/g cellulose surface charge for CNC15 is comparable to those reported on sulfuric acid hydrolyzed wood pulp (Beck-Candanedo et al., 2005). The ζ values of rice straw CNCs (−66.7 to −57.3 mV) are more negative than that of sulfuric acid hydrolyzed wood pulp CNCs (−42 mV) (Dorris & Gray, 2012). However, what this ζ value difference between rice straw and wood pulp CNCs means is unclear as neither the hydrolysis nor analysis conditions of the latter were reported. The 1.32 mmol/g surface charge of CNF-T is slightly higher than the reported values for TEMPO oxidized wood pulp, i.e., 1.12 mmol/g cellulose for never-dried kraft pulp (5 mmol/g NaClO/cellulose) (Li & Renneckar, 2011), 1.23 and 1.30 mmol/g cellulose for never-dried and dried sulfite pulp (3.8 mmol/g NaClO/cellulose) (Saito et al., 2006). The ζ of CNF-Ts (−113.3 mV) is higher than that reported (−75 mV) for various cellulose sources TEMPO oxidized with twice amount of NaClO (10 mmol/g NaClO/cellulose) (Okita, Saito, & Isogai, 2010). The surface charges and ζ values of rice straw CNCs and CNF-Ts are slightly higher than those derived under similar conditions from various wood pulps, suggesting possibly more accessibility of these chemical agents in rice straw cellulose and/or different inter-crystalline structure between these feedstock.

3.4. Morphologies of self-assembled nanocellulose

Rapid freezing dilute aqueous nanocellulose suspensions in liquid nitrogen followed by freeze-drying produced white and fluffy fibrous mass. The freeze-dried CNC15 showed many aggregated nanoparticles stringed together among sub-micron wide, irregularly shaped fibers and thin film pieces (Fig. 4a). The diameters of most nanoparticles (Fig. 4b) were between 20 and 50 nm, well above the 2 nm nanoparticles of CNC15 observed by AFM, indicative of aggregation of these nanoparticles from rapid freezing. The widths of fibers and thin films assembled from CNC15 varied greatly from 300 nm to micrometers, likely a result of the bimodally sized nanoroads. Self-assembled CNC45 solids consisted mainly ultra-fine fibers with some thin films (Fig. 4c), but no nanoparticles as seen in CNC15. The average width of self-assembled CNC45 fibers was 440 ± 127 nm, comparable to that previous reported (386 ± 125 nm) (Lu & Hsieh, 2012). The slightly wider fibers could be due the higher 0.1% CNC concentration used in this study than the previous 0.06%. Self-assembled CNC60 consisted nearly all ultra-fine fibers, averaged 346 ± 139 nm wide, but hardly any thin films (Fig. 4d). The self-assembled morphologies from freezing and freeze-drying appeared to depend on CNC sizes and their size distributions, i.e., the smallest CNC60 (average 3.92 nm wide and 116.6 nm long) assembling into ultra-fine fibers whereas the larger CNC45 (average 4.72 nm wide and 143.3 nm long) forming ultra-fine fibers as well as thin films. The nanoparticles and bimodally sized CNC15 nanorods freeze-dried into the most heterogeneous forms of nanoparticle clusters, ultra-fine fibers as well as thin films. Generally, the self-assembled fibrils increased in sizes with increasing CNC sizes. The negative charged sulfate groups provide repulsive forces to counter the association and self-assembly of CNCs. As CNC size increases, the lowered specific surface contributes to proportionally less repulsive force, enabling nanorods to associate and self-assemble to wider fibrils or even thin films.

The self-assembled CNF-B consisted ultra-fine, long and well aligned fibers with 153 ± 60 nm widths (Fig. 4e), much finer than those from CNC45 (440 ± 127 nm) and CNC60 (346 ± 139 nm). In contrast, the self-assembled CNF-T contained many thin ribbon-like pieces that were more than several microns wide among much fewer long sub-micron wide (419 ± 108 nm) fibers, similar in width

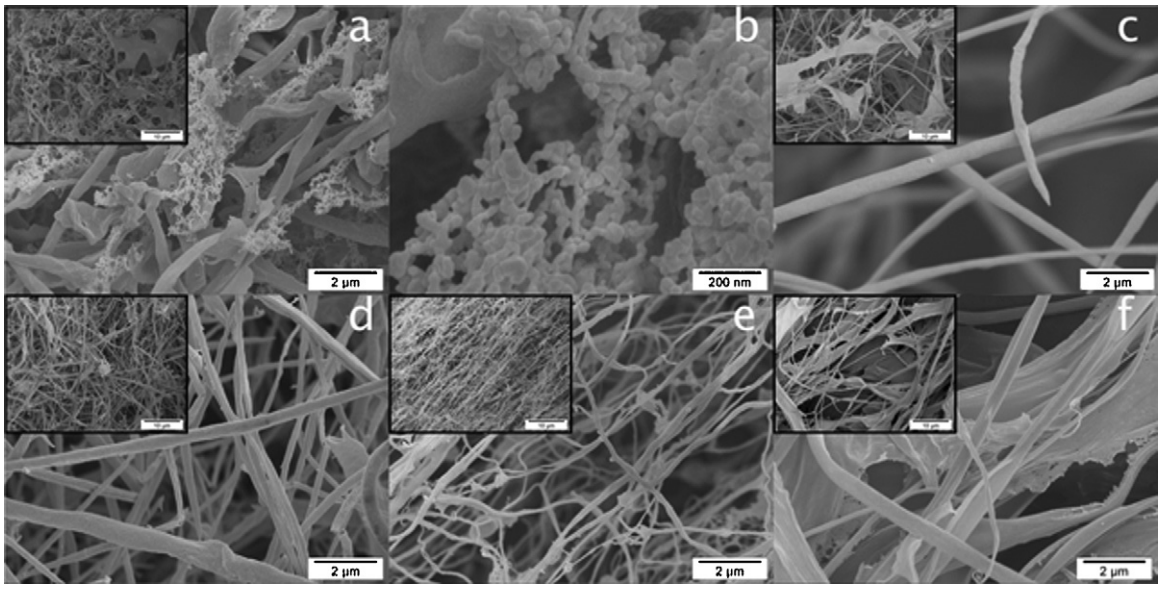

Fig. 4. SEM images of self-assembled CNC15 (a,b), CNC45 (c), CNC60 (d), CNF-B (e) and CNF-T (f).

to those from CNC45 and CNC60 (Fig. 4f). In comparison to the self-assembled CNF-Bs, the more heterogeneous fiber-ribbon and larger thin pieces assembled from CNF-Ts may be interpreted from both fibril dimensions and surface carboxyl groups. While both CNFs are micrometer long, CNF-Ts are finer (1.7 nm wide) and more uniform in widths than CNF-B (2–12 nm wide). With smaller fibril width, CNF-T has higher flexibility, specific surface and more surface hydroxyl groups to not only pack more closely together, but also hydrogen bond with each other than CNF-Bs. Furthermore, TEMPO-mediated oxidation also produce surface C6 carboxyls. The carbonyl and hydroxyl double dipoles of the CNF-T carboxyls have higher hydrogen bonding capabilities than the single dipole of the CNF-B hydroxyls. The smaller and more uniform lateral dimension, higher specific surface and the presence of stronger carboxyl dipoles of CNF-T are kinetically and thermodynamically favorable to self-assemble into more heterogeneous forms.

The major characteristics and freezing and freeze-drying induced self-assembled morphologies of rice straw nanocellulose are summarized in Table 1. For rod-like CNCs decorated with negatively charged surface sufate groups, the self-assembled morphologies depend highly on their dimensions and dimesional uniformity, showing the smallest and more uniform CNC60 assembled into exclusively ultra-fine (346 ± 139 nm) fibers while the larger and more heterogeneously sized CNCs assembled into some ultra-fine fibers as well as other irregular forms of aggregated nanoparticles and thin films. Self-assembling of the longer CNFs, on the other hand, depends primarily on their lateral dimensions and surface chemistries, less on dimensional uniformity. The uncharged CNF-Bs, even though larger and more dimensionally heterogeneous, assembled into most uniform and finest (153 ± 60 nm) fibers; while thinnest and most uniform CNF-Ts with aboundant surface carboxyls assembled into heterogeneous morphologies containing thin ribbon-like films in addition to ultra-fine (419 ± 108 nm) fibers.

In isolating CNFs by high-speed blending and TEMPO mediated oxidation, larger cellulose fibers (CFs) were also recovered as sediments from centrifugation, accounting for 88% (CF-B) and 80% (CF-T) of the original cellulose, respectively. CF-B and CF-T were showed to be mostly 100 μm or longer microfibers of similar average diameters of 5.13 ± 2.63 μm and 5.56 ± 1.83 μm, respectively (Fig. 5a and c). Some much finer sub-micron fibrils were also observed with CF-B (Fig. 5a), which could be CNF-Bs trapped among CF-B. Freeze-drying both dilute CF susptensions also produced white fluffy fibrous mass, similar to their freeze-dried CNF and CNC counterparts. The freeze-dried CF-B consisted of thin film pieces inter-laced with sub-micron wide fibrils (Fig. 5b), the latter appearing more abundant than the air-dried CF-B (Fig. 5a). During rapid freezing and freeze-drying, the nanometer-wide CNF-B self-assembled into to sub-micron wide fibers (Fig. 4e) whereas the micron-wide CF-B mostly assembled into tens of micrometer wide thin films, both showing self-assembling behavior, but at different scale levels. CF-T freeze-dried into thin films (Fig. 5d) among

Table 1
Rice straw nanocellulose characteristics and self-assembled morphologies.

Nano-cellulose	CNC/CNF characteristics[a]				Assembled morphologies	
	Yield (%)	Thickness (nm)	Length (nm)	zeta potential (mV)	Fiber width[c] (nm)	Others
CNC15[b]	16.9	2.13 ± 0.72 6.74 ± 1.84	68.6 ± 16.6 165.6 ± 42.0	−66.7 ± 0.3	Highly variable, 300 nm to submicron	Aggregated nanoparticles (20–50 nm wide); thin films (over several microns wide)
CNC45	6.8	4.72 ± 1.25	143.3 ± 30.9 143.3 ± 30.9	−57.3 ± 2.7	440 ± 127	Thin films (over several microns wide)
CNC60	4.9	3.96 ± 1.32	116.6 ± 27.6	−63.8 ± 2.2	346 ± 139	N/A
CNF-B	12	2.70 ± 1.22 8.46 ± 4.14	100–200 $>10^3$	NA	153 ± 60	N/A
CNF-T[b]	19.7	1.73 ± 0.56	10^2 to 10^3	−113.3 ± 1.5	419 ± 108	Thin films (over several microns wide)

[a] Thickness by AFM; lengths by TEM.
[b] CNC15 and CNF-T have surface charges of 0.29 and 1.32 mmol/g cellulose, respectively.
[c] Fiber width of self-assembler fibers by SEM.

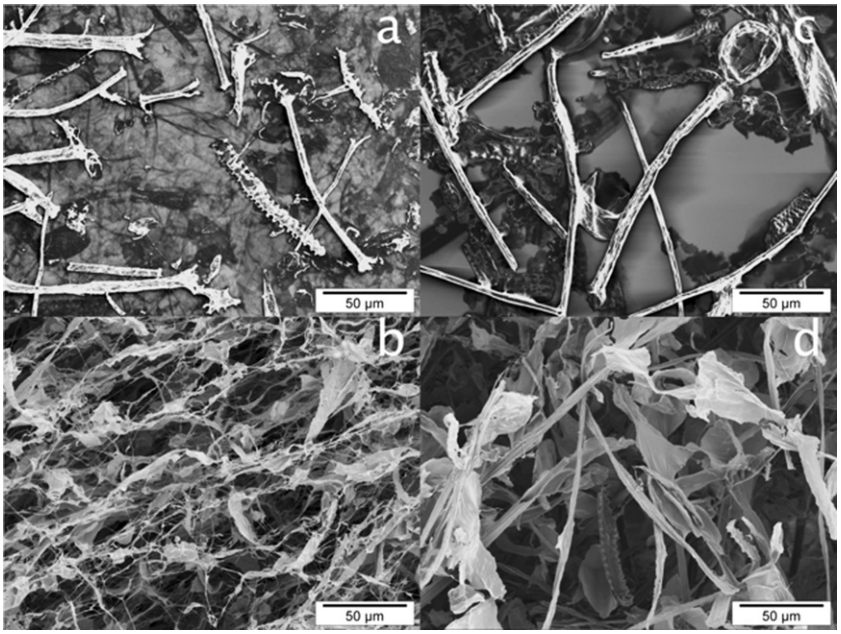

Fig. 5. SEM images of air-dried (a,c) and freeze-dried (b,d) cellulose fibers: (a) air-dried CF-B, (b) freeze-dried CF-B, (c) air-dried CF-T, (d) freeze-dried CF-T.

undefibrillated microfibers as observed on the air-dried CF-T (Fig. 5c).

Freezing dilute aqueous nanocellulose suspensnions with liquid nitrogen (−196 °C) and freeze-drying have shown to cause self-assembling of nanocellulose to form white and fluffy fibrous mass containing sub-micron wide and hundreds of micrometer long fibers in all cases. The dimensions of the self-assembled fibers vary with nanocellulose dimensions and surface characteristics, long CNFs without surface charges from mechanical blending assembled into the thinnest (153 ± 60 nm) and most uniform fibrous structures. Rapid freezing at −196 °C causes free water in the dilute nanocellulose suspensions to form ice crystals, concentrating nanocellulose to closer contact with each other in both lateral and axial directions. In the much slower freeze-drying process that follows, the closely packed nanocellulose self-assembles into sub-micron wide and micrometer long fibers as well as other more heterogeneous ribbons and thin films, influenced by their dimensional and surface characteristics and facilitated by inter-fibrilliar attraction via hydrogen bonding among the abundant surface hydroxyls and carboxyls. Sublimation of ice crystals leaves pores among the various particulates, fibers and films. Both fibrillar morphologies and assoicated inter-fibrillar pore structures may be further exploited to generate new fibrillar network structures and porous materials.

3.5. Chemical and crystalline structures of self-assembled nanocellulose

Self-assembled CNC45, CNF-B and CNF-T showed the same cellulose characteristic FTIR peaks, i.e., O—H, CH and C—O stretching vibrations at 3400 cm^{-1}, 2900 cm^{-1} and 1060 cm^{-1}, respectively as pure rice straw cellulose (Fig. 6a). The peak at 1640 cm^{-1} associated with the O—H bending vibration of absorbed water was evident in spectra of cellulose, CNC45 and CNF-B whereas CNF-T showed a more pronounced peak at 1619 cm^{-1}, likely from asymmetrical carboxylate COO^- vibration at 1610 cm^{-1} overlapping with the O—H bending vibration of the absorbed water. The small peak at 897 cm^{-1} in the anomeric region (950–700 cm^{-1}), representing the glycosidic $-C_1-O-C_4$ deformation characteristic of the β-glycosidic link in cellulose, appeared weaker for CNF-B and CNF-T, indicating a scission of β-glycosidic bond by these mechanical and chemical treatments. Essentially, CNCs and CNFs isolated by mechanical or acid hydrolysis showed little chemical alteration that is observable by FTIR while the C6 carboxylates on CNF-T from

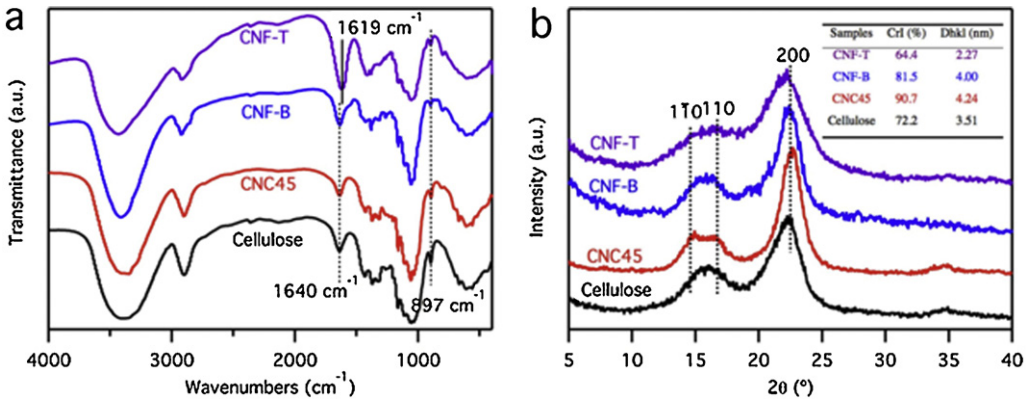

Fig. 6. (a) FTIR and (b) XRD spectra of rice straw cellulose and self-assembled nanocellulose. Inset table in b is crystallinity index and crystallite dimension.

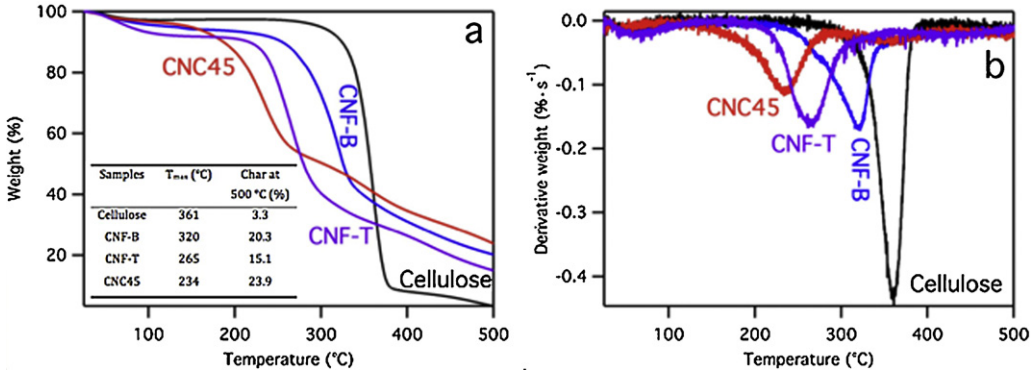

Fig. 7. Thermal analysis of rice straw cellulose and self-assembled nanocellulose: (a) TGA and (b) DTG curves. Inset table is maximum degradation temperature (T_{max}) and char residues at 500 °C.

TEMPO-mediated oxidation were abundant enough to be clearly detected.

All three self-assembled nanocellulose solids also showed the same X-ray diffraction (XRD) as pure rice straw cellulose with cellulose Iβ characteristic peaks at $2\theta = 14.7°$, 16.8° and 22.7° (Fig. 6b), representing the $1\bar{1}0$, 110, and 200 crystallographic planes of the monoclinic cellulose I lattice, respectively. The XRD of CNC45 exhibited the most intense 200 peak and most resolved $1\bar{1}0$ and 110 peaks whereas that of CNF-B was most similar to pure rice cellulose. On the other hand, CNF-T had the broadest and least defined XRD peaks, a clear indication of lower crystallinity.

The crystallinity index (*CrI*) and crystallite dimension calculated from XRD patterns of pure rice straw cellulose were 72.2%, and 3.51 nm, respectively (Inset, Fig. 6b). Mechanical defibrillation by blending produced CNF-B with a higher *CrI* of 81.5% whereas CNC45 isolated by sulfuric acid hydrolysis had an even higher 90.7% *CrI*. The crystallite sizes also increased to 4.00 nm and 4.24 nm for CNF-B and CNC45, respectively. TEMPO oxidation, on the other hand, lowered the CrI and crystallite size of CNF-T considerably to 64.4% and 2.27 nm, respectively. Although TEMPO oxidized cellulose from various sources have been previously reported to show unchanged crystallinity and crystallite size (Saito & Isogai, 2004), it is unclear if that observation was made on the entire oxidized products which could contain un-oxidized original cellulose amongst TEMPO-oxidized cellulose. In this study, the TEMPO oxidized rice straw cellulose was separated from un-oxidized and less oxidized cellulose thus represented mainly the oxidized nanocellulose. The higher yield and lower *CrI* and crystallite size of CNF-T show the selective TEMPO-mediated oxidation, i.e., on C6 hydroxyls only, facilitated mechanical defibrillation of most CNFs. The average CNF-T width of 1.7 nm is much smaller than the original rice straw cellulose crystallites size (3.51 nm), suggesting oxidizing reagents possibly penetrating into the crystallites. This aspect would require further investigation. These self-assembled nanocellulose has not only retained the cellulose Iβ crystalline structure, but exhibited superior crystallinity in the case of sulfuric acid hydrolysis (90.7% CrI for CNC45) and mechanical defibrillation (81.5% CrI for CNF-B) and significant retention of crystallinity from TEMPO oxidation (64.4% CrI for CNF-T) when compared to the 72.2% CrI of the original pure rice cellulose.

3.6. Thermal stability of self-assembled nanocellulose

Pure rice straw cellulose was observed to decompose in the 280–380 °C region whereas self-assembled CNF-B, CNF-T and CNC45 decomposed at significantly lowered temperature ranges of 235–350 °C, 210–310 °C and 160–280 °C, respectively (Fig. 7a). Consistent with the onset degradation temperature, maximum degradation temperatures (T_{max}) of self-assembled CNF-B, CNF-T and CNC45 were also lowered to 320 °C, 265 °C and 234 °C, respectively, from that of rice straw cellulose (361 °C) (Inset, Fig. 7a). Lowered degradation temperature of CNF-B could be due to the smaller fiber dimensions (153 nm) as compared to the macroscopic cellulose fibers, which lead to higher surface areas exposing to heat. Additionally, surface carboxyl groups and sulfate groups are expected to cause the lowered degradation temperature for CNF-T and CNC45 by either direct solid-to-gas phase transitions from decarboxylation of surface carboxyl groups (Fukuzumi, Saito, Wata, Kumamoto, & Isogai, 2009; Fukuzumi, Saito, Okita, & Isogai, 2010), or lowered activation energy of decomposition from the surface sulfate groups (Lu & Hsieh, 2010; Roman & Winter, 2004). Despite reduced thermal stability, these self-assembled CNF-T, CNF-B and CNC45 showed much higher char residues of 15.1, 20.3 and 23.9%, respectively, more than four to seven times of that from the original rice straw cellulose (3.3%). Theoretically, ideal pyrolysis of cellulose should yield 44.4% of carbonaceous residues if all hydrogen and oxygen are released as H_2O through dehydration reaction. However, cellulose pyrolysis contains other complex reactions including decarbonylation to CO, decarboxylation to CO_2, as well as reactions to form other gaseous products, such as H_2 and CH_4, etc. Increased char residues have been observed on CNCs from bacteria cellulose (Roman & Winter, 2004), cotton (Lu & Hsieh, 2010) as well as wood (Wang, Ding, & Cheng, 2007) and have been ascribed to the dehydration effect of the sulfate group (Kim, Nishiyama, Wada, & Kuga, 2001; Wang et al., 2007). The high char yields for all self-assembled nanocellulose may be due to the favored dehydration reaction at lower temperature. In addition, decomposition of these self-assembled nanocellulose would require less thermal energy and occur at lower temperature due to their smaller lateral dimensions, as manifested from the lower degradation temperature.

4. Conclusion

Nanocellulose has been isolated from rice straw via sulfuric acid hydrolysis, mechanical blending and TEMPO oxidation to distinct morphologies and surface properties. Sulfuric acid hydrolysis isolated CNCs in decreasing sizes and yields with increasing time. CNC45 were more uniform in dimensions (4.7 nm wide and 143 nm long) and reasonable in yield (6.8%) whereas the highest yielded CNC15 contained both nanoparticles and nanorods with bimodally distributed sizes. CNF-Bs produced by high-speed blending were bimodally distributed in dimensions, i.e., 2.7 nm wide and 100–200 nm long as well as 8.5 nm wide and several micrometers long, at a 12% yield. Also micrometers long, CNF-Ts generated via TEMPO oxidation were the finest (1.7 nm wide), most uniform in

widths and highest in yield (19.7%). All CNCs contained similar surface sulfate and were similarly negative charged (−67 to −57 mV) irrespective of hydrolysis time while CNF-Ts were far more polar and negatively charged (1.32 mmol/g cellulose, −113.3 mV) than CNCs (0.29 mmol/g cellulose), evident of significant amount of surface carboxyl groups. Nanocellulose suspensions self-assembled into white and fluffy fibrous mass through rapid freezing in liquid nitrogen and freeze-drying. Morphologies of self-assembled CNC depended on their sizes and size distribution: the more uniformly sized CNC45 and CNC60 assembled into sub-micrometer fibers with 440 nm and 346 nm average widths, respectively, whereas the more heterogeneously sized CNC15 assembled into heterogeneous collections of aggregated nanoparticles, sub-micrometer wide fibers, and micrometer wide thin films. In contrast, self-assembled CNFs morphologies showed less dependence on their dimensional uniformity, but more on surface chemistries: the chemically homogeneous and uncharged CNF-Bs, although bimodally distributed in sizes, self-assembled into finest fibers with average width of 153 nm whereas the highly charged CNF-Ts with strongly dipolar carboxyls assembled into both sub-micrometer wide fibers and micrometer wide thin films. All self-assembled nanocellulose retained cellulose Iβ structure with superior crystallinities, i.e., varying from 64.4% CrI for CNF-T, 81.5% CrI for CNF-B to the highest 90.7% CrI for CNC45. Self-assembled nanocellulose decomposed at lower onset temperature, but retained more than four to seven times of char residues than pure cellulose precursor, manifesting altered decomposition mechanisms. The self-assembling behavior of nanocellulose has demonstrated this cryogenic drying approach to be an attractive alternative to generate sub-micrometer sized cellulose fibers with highly crystalline cellulose Iβ structure that could surpass its source. Self-assembling of nanocellulose driven by super fast freezing of water and association via hydrogen bonding results in not only distinctively different fibrillar morphologies, but also inter-fibrillar pores, both may be further exploited for new physical and chemical structures and properties.

Acknowledgments

Financial support for this research from the California Rice Research Board (Project RU-9) is greatly appreciated

Appendix A. Supplementary data

Supplementary data associated with this article can be found, in the online version, at http://dx.doi.org/10.1016/j.carbpol.2013.02.022.

References

Abe, K., & Yano, H. (2009). Comparison of the characteristics of cellulose microfibril aggregates of wood, rice straw and potato tuber. *Cellulose*, *16*(6), 1017–1023.

Alemdar, A., & Sain, M. (2008). Isolation and characterization of nanofibers from agricultural residues – Wheat straw and soy hulls. *Bioresource Technology*, *99*(6), 1664–1671.

Beck-Candanedo, S., Roman, M., & Gray, D. G. (2005). Effect of reaction conditions on the properties and behavior of wood cellulose nanocrystal suspensions. *Biomacromolecules*, *6*(2), 1048–1054.

Bondeson, D., Mathew, A., & Oksman, K. (2006). Optimization of the isolation of nanocrystals from microcrystalline cellulose by acid hydrolysis. *Cellulose*, *13*(2), 171–180.

Chen, W. S., Yu, H. P., & Liu, Y. X. (2011). Preparation of millimeter-long cellulose I nanofibers with diameters of 30–80 nm from bamboo fibers. *Carbohydrate Polymers*, *86*(2), 453–461.

Dong, S. P., & Roman, M. (2007). Fluorescently labeled cellulose nanocrystals for bioimaging applications. *Journal of the American Chemical Society*, *129*(45), 13810

Dorris, A., & Gray, D. G. (2012). Gelation of cellulose nanocrystal suspension in glycerol. *Cellulose*.

Elazzouzi-Hafraoui, S., Nishiyama, Y., Putaux, J. L., Heux, L., Dubreuil, F., & Rochas, C. (2008). The shape and size distribution of crystalline nanoparticles prepared by acid hydrolysis of native cellulose. *Biomacromolecules*, *9*(1), 57–65.

Fukuzumi, H., Saito, T., Okita, Y., & Isogai, A. (2010). Thermal stabilization of TEMPO-oxidized cellulose. *Polymer Degradation and Stability*, *95*(9), 1502–1508.

Fukuzumi, H., Saito, T., Wata, T., Kumamoto, Y., & Isogai, A. (2009). Transparent and high gas barrier films of cellulose nanofibers prepared by TEMPO-mediated oxidation. *Biomacromolecules*, *10*(1), 162–165.

Habibi, Y., Lucia, L. A., & Rojas, O. J. (2010). Cellulose nanocrystals: chemistry self-assembly, and applications. *Chemical Reviews*, *110*(6), 3479–3500.

Heath, L., & Thielemans, W. (2010). Cellulose nanowhisker aerogels. *Green Chemistry*, *12*(8), 1448–1453.

Isogai, A., Saito, T., & Fukuzumi, H. (2011). TEMPO-oxidized cellulose nanofibers. *Nanoscale*, *3*(1), 71–85.

Iwamoto, S., Kai, W. H., Isogai, A., & Iwata, T. (2009). Elastic modulus of single cellulose microfibrils from tunicate measured by atomic force microscopy. *Biomacromolecules*, *10*(9), 2571–2576.

Iwamoto, S., Nakagaito, A. N., & Yano, H. (2007). Nano-fibrillation of pulp fibers for the processing of transparent nanocomposites. *Applied Physics A: Materials Science & Processing*, *89*(2), 461–466.

Jiang, F., Esker, A. R., & Roman, M. (2010). Acid-catalyzed and solvolytic desulfation of H2SO4-hydrolyzed cellulose nanocrystals. *Langmuir*, *26*(23), 17919–17925.

Kim, D. Y., Nishiyama, Y., Wada, M., & Kuga, S. (2001). High-yield carbonization of cellulose by sulfuric acid impregnation. *Cellulose*, *8*(1), 29–33.

Klemm, D., Heublein, B., Fink, H. P., & Bohn, A. (2005). Cellulose: Fascinating biopolymer and sustainable raw material. *Angewandte Chemie: International Edition*, *44*(22), 3358–3393.

Li, Q. Q., & Renneckar, S. (2011). Supramolecular Structure characterization of molecularly thin cellulose I nanoparticles. *Biomacromolecules*, *12*(3), 650–659.

Liu, H. Q., & Hsieh, Y. L. (2002). Ultrafine fibrous cellulose membranes from electrospinning of cellulose acetate. *Journal of Polymer Science Part B: Polymer Physics*, *40*(18), 2119–2129.

Lu, P., & Hsieh, Y. L. (2010). Preparation and properties of cellulose nanocrystals: Rods, spheres, and network. *Carbohydrate Polymers*, *82*(2), 329–336.

Lu, P., & Hsieh, Y. L. (2012). Preparation and characterization of cellulose nanocrystals from rice straw. *Carbohydrate Polymers*, *87*(1), 564–573.

Nickerson, R. F., & Habrle, J. A. (1947). Cellulose intercrystalline structure. *Industrial & Engineering Chemistry*, *39*(11), 1507–1512.

Nishino, T., Matsuda, I., & Hirao, K. (2004). All-cellulose composite. *Macromolecules*, *37*(20), 7683–7687.

Okita, Y., Saito, T., & Isogai, A. (2010). Entire surface oxidation of various cellulose microfibrils by TEMPO-mediated oxidation. *Biomacromolecules*, *11*(6), 1696–1700.

Roman, M., & Winter, W. T. (2004). Effect of sulfate groups from sulfuric acid hydrolysis on the thermal degradation behavior of bacterial cellulose. *Biomacromolecules*, *5*(5), 1671–1677.

Sadeghifar, H., Filpponen, I., Clarke, S. P., Brougham, D. F., & Argyropoulos, D. S. (2011). Production of cellulose nanocrystals using hydrobromic acid and click reactions on their surface. *Journal of Materials Science*, *46*(22), 7344–7355.

Saito, T., & Isogai, A. (2004). TEMPO-mediated oxidation of native cellulose. The effect of oxidation conditions on chemical and crystal structures of the water-insoluble fractions. *Biomacromolecules*, *5*(5), 1983–1989.

Saito, T., Kimura, S., Nishiyama, Y., & Isogai, A. (2007). Cellulose nanofibers prepared by TEMPO-mediated oxidation of native cellulose. *Biomacromolecules*, *8*(8), 2485–2491.

Saito, T., Nishiyama, Y., Putaux, J. L., Vignon, M., & Isogai, A. (2006). Homogeneous suspensions of individualized microfibrils from TEMPO-catalyzed oxidation of native cellulose. *Biomacromolecules*, *7*(6), 1687–1691.

Saito, T., Uematsu, T., Kimura, S., Enomae, T., & Isogai, A. (2011). Self-aligned integration of native cellulose nanofibrils towards producing diverse bulk materials. *Soft Matter*, *7*(19), 8804–8809.

Scherrer, P. (1918). Estimation of the size and internal structure of colloidal particles by means of Röntgen rays. *Nachrichten von der Gesellschaft der Wissenschaften zu Göttingen*, 96–100.

Segal, L., Creely, J. J., Martin, A. E., Jr., & Conrad, C. M. (1959). An empirical method for estimating the degree of crystallinity of native cellulose using the X-ray diffractometer. *Textile Research Journal*, *29*, 786–794.

Siro, I., & Plackett, D. (2010). Microfibrillated cellulose and new nanocomposite materials: A review. *Cellulose*, *17*(3), 459–494.

Uetani, K., & Yano, H. (2011). Nanofibrillation of Wood Pulp Using a High-Speed Blender. *Biomacromolecules*, *12*(2), 348–353.

Uetani, K., & Yano, H. (2012). Zeta potential time dependence reveals the swelling dynamics of wood cellulose nanofibrils. *Langmuir*, *28*(1), 818–827.

Wang, N., Ding, E. Y., & Cheng, R. S. (2007). Thermal degradation behaviors of spherical cellulose nanocrystals with sulfate groups. *Polymer*, *48*(12), 3486–3493.

Zimmermann, T., Bordeanu, N., & Strub, E. (2010). Properties of nanofibrillated cellulose from different raw materials and its reinforcement potential. *Carbohydrate Polymers*, *79*(4), 1086–1093.

Zuluaga, R., Putaux, J. L., Restrepo, A., Mondragon, I., & Ganan, P. (2007). Cellulose microfibrils from banana farming residues: isolation and characterization. *Cellulose*, *14*(6), 585–592.